NANOSYSTEMS: PHYSICS, CHEMISTRY, MATHEMATICS, 2020, 11 (4), P. 474–479

The effect of MgO additive on the g-C_3N_4 performance in electrochemical reforming of water-ethanol solution

M. I. Chebanenko[1,*], K. D. Martinson[1], I. V. Matsukevich[2], V. I. Popkov[1]

[1]Ioffe Institute, St. Petersburg, 194021, Russia

[2]Institute of General and Inorganic Chemistry of the National Academy of Sciences of Belarus, Minsk BY-220072, Republic of Belarus

*m_chebanenko@list.ru

PACS 82.45.Yz **DOI 10.17586/2220-8054-2020-11-4-474-479**

In this work, a simple wet-chemical route was proposed to synthesize g-C_3N_4/MgO (5% wt.) with enhanced electrocatalytic activity toward hydrogen evolution from water-ethanol (10% vol.) solution. It was found that synthesized nanocomposite is a single phase and chemically pure, consisting of graphitic carbon nitride (g-C_3N_4) and cubic magnesium oxide (MgO, periclase) with an average crystallite size of 15.5 nm and 9.5 nm, respectively. It was shown that magnesia nanoparticles are evenly distributed on the surface of g-C_3N_4 nanosheets and uniform distribution of components is observed over the nanocomposite volume. It was found that this feature leads to an improvement in the electrocatalytic characteristics of the synthesized nanocomposite. So, the g-C_3N_4/MgO-coated electrode has an overpotential of -251 mV, which is better than for a g-C_3N_4-coated (-264 mV) or pure nickel (-293 mV) electrode. Moreover, the nanocomposite-based electrode posses a low Tafel slope (-106.7 mV/dec) and high cyclic and chronopotentiometry stability.

Keywords: graphitic carbon nitride, magnesia, nanopowders, electrocatalytic reforming, hydrogen evolution reaction.

Received: 8 June 2020

Revised: 16 July 2020

1. Introduction

Currently, the production of hydrogen using photo- and electrocatalytic conversion of solar energy into chemical energy seems to be a rather promising solution for main problems associated with environmental and energy crises [1]. The key task, in this case, is the search for an inexpensive and effective photo- and electrocatalysts exhibiting activity under the influence of visible light and effective electron transfer. Among them, the graphite-like carbon nitride (g-C_3N_4) stands out, which is a semiconductor with high stability, and photo- and electrocatalytic activity [2–4]. At the same time, in its pure form, graphite-like carbon nitride is characterized by a low specific surface area, a lack of active centers on its surface, rapid recombination of photogenerated electron-hole pairs, and a wide bandgap (2.7 eV), which all together causes insufficiently high photo- and electrocatalytic activity [5, 6].

But the synthesis of heterogeneous structures based on graphite-like carbon nitride and some oxide can neutralize the disadvantages mentioned above. For example, it was shown that the preparation of the g-C_3N_4/MgO nanocomposite allows one to achieve a high rate of hydrogen evolution – up to 30.1 μmol/h in the photoinduced hydrogen evolution reaction (HER) process, which is almost 6 times higher than for pure graphite-like carbon nitride [7]. The authors explain this by the fact that in this case, the presence of a heterojunction possesses quick transfer of photoinduced electrons from the conduction band of g-C_3N_4 to the conduction band of MgO, which contributes to a significant separation of photoinduced electrons and holes and effectively suppresses the recombination of electron-hole pairs. Moreover, it can be assumed that the intercalation of magnesium oxide into the interlayer space of graphite-like carbon nitride may lead to the enhanced specific surface area providing higher catalytic activity of obtained nanocomposite.

However, another important direction of hydrogen production is through the electrocatalytic reforming of aqueous-ethanol solutions using catalysts based on graphite-like carbon nitride nanocomposites is still largely unexplored. In the case of g-C_3N_4/MgO nanocomposite, the mesoporous g-C_3N_4 can be tuned by different amounts of MgO to significantly enhance its electrocatalytic performance and reduce the absolute value of its overpotential. However, previously it was shown that an excessive amount of second component (MgO) may also decrease the activity and stability of g-C_3N_4 [8]. Based on this work 5 wt%. can be considered as optimal MgO content for g-C_3N_4/MgO electrocatalyst production. Thus, this work aimed to synthesize and complex study the structural, morphological, and electrochemical features of the g-C_3N_4/MgO nanocomposite. A simple wet-chemistry technique is proposed to synthesize a nanocomposite of graphitic carbon nitride and magnesium oxide as a promising material for hydrogen production from water-ethanol solution. A comprehensive study of the structure and morphology of g-C_3N_4/MgO was

carried out using the complex physicochemical analysis to better understand the origin of its enhanced electrocatalytic activity.

2. Experimental section

2.1. Synthesis procedure

The nanopowder of the initial graphitic carbon nitride (g-C_3N_4) was synthesized by heat treatment of urea ($(NH_2)_2CO$) under aerobic conditions. A detailed description of its synthesis procedure and preparation of a g-C_3N_4-based colloidal solution was previously given in [9, 10]. After homogenization, 1.5 mg of magnesium acetate tetrahydrate ($Mg(CH_3COO)_2{\cdot}4H_2O$ or $Mg(Ac)_2{\cdot}4H_2O$) was dissolved in 10 ml of distilled water using magnetic stirring. The mixture then was evaporated at 100°C and calcined at 350°C for 30 minutes followed by grinding. As a result, initial g-C_3N_4 powder and g-C_3N_4/MgO nanocomposite (mass fraction of magnesia is 5%) were prepared. MgO to g-C_3N_4 proportion was selected based on [8] work. The generalized synthesis scheme of both g-C_3N_4 and g-C_3N_4/MgO shown in Fig. 1. All the chemicals used were of analytical grade.

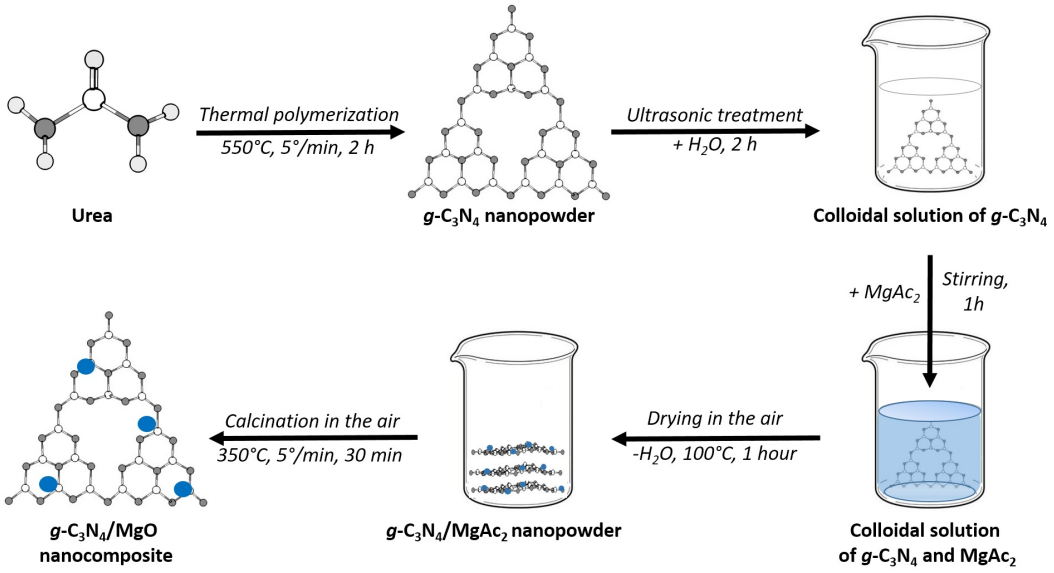

FIG. 1. Schematic representation of the synthesis procedure for g-C_3N_4 and g-C_3N_4/MgO nanopowders

2.2. Physicochemical characterization

The elemental composition and morphology of the synthesized samples were studied by energy-dispersive X-ray spectroscopy (EDS) and scanning electron microscopy (SEM) using Tescan Vega 3 SBH scanning electron microscope equipped with an Oxford INCA x-act X-ray microanalysis device. An Oxford Instruments INCA system was used for chemical analysis, including both line scan EDS and elemental mapping utilizing a 10 nm probe size. All concentration profiles were plotted using elements percentage. SEM-images of the samples were acquired in both SE (morphological contrast) and BSE (phase contrast) modes. X-ray phase analysis was performed on a Rigaku SmartLab 3 X-ray powder diffractometer (CuKα radiation, $\lambda = 0.154051$ nm, Bragg angle range 10–80°), phase analysis of the compositions was performed using JCPDS PDF-2 database. The average crystallite size (coherent-scattering regions) was calculated from the broadening of X-ray diffraction lines using the fundamental parameter method implemented in the SmartLab Studio II software.

2.3. Electrocatalytic performance

The electrochemical measurements were carried out on Elins P20X potentiostat using a three-electrode cell. The working electrode was a nickel (Ni) substrate used as a reference or initial g-C_3N_4 and g-C_3N_4/MgO nanocomposite deposited on a Ni substrate as a suspension from a 0.5% solution of Nafion in isopropyl alcohol. Ag/AgCl and platinum electrodes were used as reference and counter electrodes, respectively. The overpotentials values were calibrated with respect to the reversible hydrogen electrode (ERHE) according to the Nernst equation. All measurements were carried out at standard conditions (T=25°C, P=1 atm.) in an aqueous solution consisting of ethanol C_2H_5OH (10% vol.) and

1M KOH (pH = 14). Cyclic CV curves were taken in the potential range from open circuit potential to 1.5 V with a sweep rate of 5-10 mV/s. Qualitatively, the working overpotential of the sample was determined from the CV curves at a current density of 10 mA/cm^2. Electrocatalytic stability of the g-C_3N_4/MgO-based electrode was additionally characterized by cyclic voltammetry (100 cycles) and chronopotentiometry (10000 s). Electrochemical measurements were performed without IR-compensation.

3. Results and discussion

The EDS investigations were performed to obtain information about the gross chemical composition of the g-C_3N_4/MgO sample. Five different areas were selected in the sample for analysis to ensure the representativeness (Fig. 2(a)). It was shown that the typical EDS spectrum contains the lines that can be assigned to Mg, O, C and N elements (Fig. 2(b)). The quantitative elemental composition of the sample in the selected areas and on average indicates its compliance with the composition planned in the synthesis. Thus, the EDS results confirm that MgO weight fraction in g-C_3N_4/MgO nanocomposite is 5% within a method error. Further, this sample will be designated as g-C_3N_4/5%MgO.

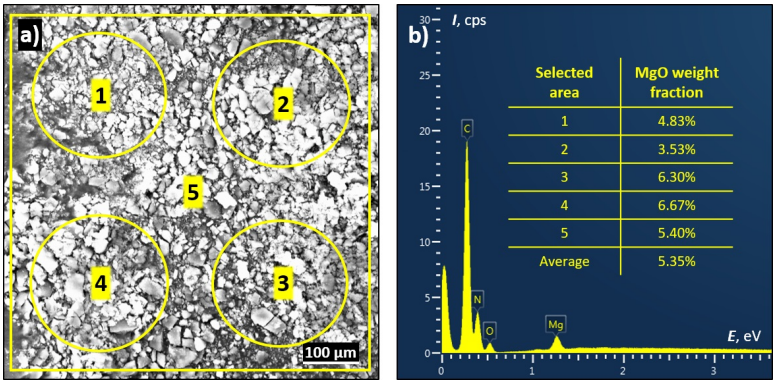

FIG. 2. Results of the selected area EDS analysis of g-C_3N_4/MgO nanocomposite: (a) SEM image of the sample and selected areas, (b) EDS spectrum of area #5. The table inset in (b) shows data on the MgO weight fraction in g-C_3N_4/MgO nanocomposite by selected areas and on average

The overview SEM image of the g-C_3N_4/MgO nanocomposite in BSE mode and the distribution of C, N, Mg and O elements on its surface are presented in Fig. 3. The BSE SEM image (Fig. 3(a)) does not show any phase contrast in the synthesized sample. The element mapping of both individual (Fig. 3(b-e)) and superposed (f) elements confirms the homogeneous distribution of all the elements in the g-C_3N_4/MgO nanocomposite without the formation of any clusters of individual MgO or g-C_3N_4 phases on a microscale.

Figure 4 shows the SEM images of g-C_3N_4/5%MgO nanocomposite at different magnification acquired in SE mode. As one can see the morphology of g-C_3N_4, which is the main component of g-C_3N_4/5%MgO nanocomposite (95% wt.), at low magnifications (Fig. 4(a,b)) is quite lumpy with a large number of micron-size aggregates. But at higher magnification (Fig. 4(c)), it becomes clear that each such aggregates consist of individual g-C_3N_4 nanosheets, some of which are gradually flaked off. Besides, in Fig. 4(b,c), it can be seen that MgO nanoparticles are also present and contrastingly differ from graphitic carbon nitride; it's clear that these nanoparticles are evenly distributed over the surface of g-C_3N_4 nanosheets. Thus, even at the nanoscale, the synthesized g-C_3N_4/5%MgO nanocomposite is characterized by a high homogeneity of the spatial distribution of the main components.

Figure 5 shows the PXRD patterns of initial g-C_3N_4 and g-C_3N_4/MgO (5%) nanocomposite. In the case of pure g-C_3N_4, there are two distinct well-defined diffraction peaks at 13.6 and 27.7 degrees, related to the (100) and (002) diffraction planes of graphitic carbon nitride (JCPDS 87-1526). The diffraction pattern of g-C_3N_4/5%MgO nanocomposite shows additional peaks located at 36.8°, 43.2°, 62.5° that can be attributed to (111), (200), (220) planes of magnesia (MgO) with periclase cubic structure (JCPDS 78-0430). As can be seen from the inset in Fig. 5, the average crystallite size of g-C_3N_4 in pure form and nanocomposite is 16.9 nm and 15.5 nm, correspondingly. This decrease in the crystallite size can be associated with the influence of magnesium oxide, which can be formed between individual g-C_3N_4 nanosheets during the synthesis and thereby lead to partial exfoliation of graphitic carbon nitride. These results also confirmed that MgO nanoparticles with an average crystallite size of 9.5 nm are preferably formed in close contact with g-C_3N_4.

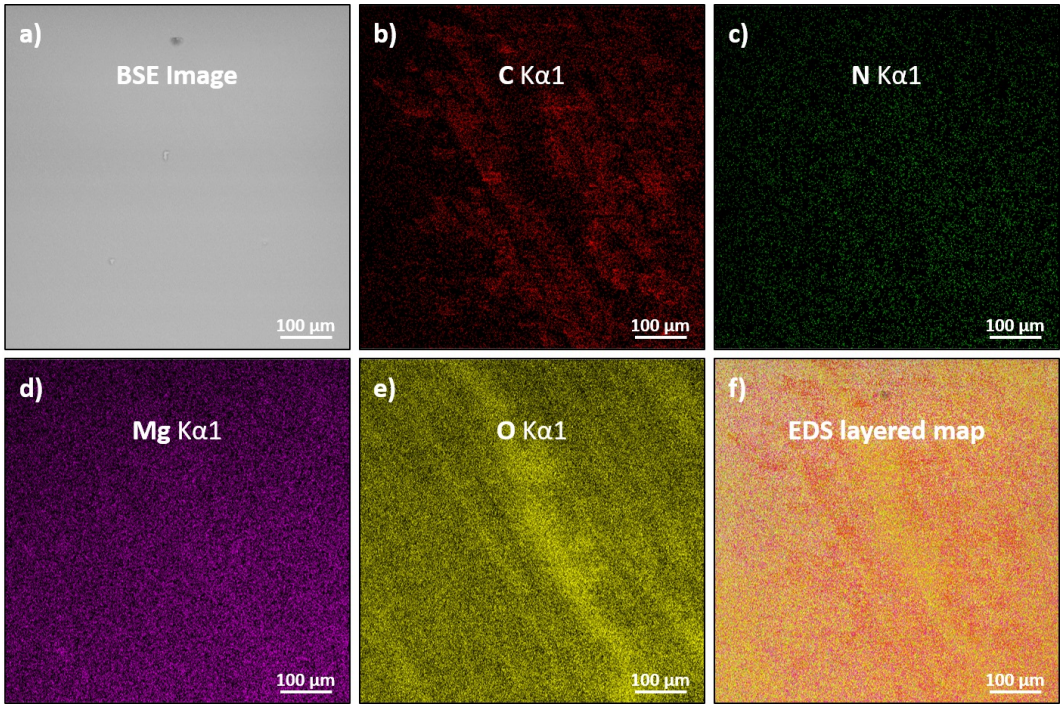

FIG. 3. EDS mapping of g-C_3N_4/5%MgO nanocomposite: (a) SEM image of the area under analysis in BSE mode, (b) carbon (C Kα1) mapping, (c) nitrogen (N Kα1) mapping, (d) magnesium (Mg Kα1) mapping, (e) oxygen (O Kα1) mapping, (f) EDS layered map as a result of (b–e) maps superposition

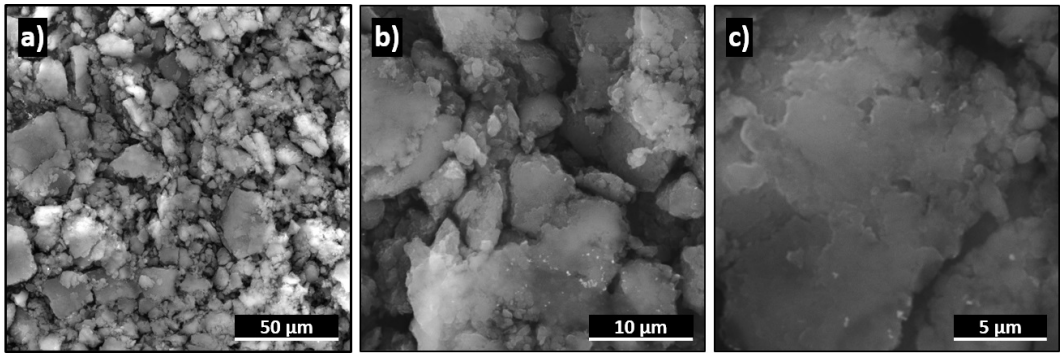

FIG. 4. SEM images of g-C_3N_4/5%MgO nanocomposite at different magnifications (a–c)

A linear potential sweep method with a constant sweep speed of 10 mV/s was used as the main measurement procedure to evaluate the electrocatalytic activity of the synthesized g-C_3N_4/5%MgO nanocomposite with respect to pure Ni substrate and initial g-C_3N_4 (Fig. 6). As shown in Fig. 6(a), the overpotential on a Ni substrate at a current density of 10 mA/cm^2 is 293 mV, which matches to the literature data [11]. In the case of g-C_3N_4 and g-C_3N_4/MgO nanocomposite, the overpotential value at the same current density is 264 and 251 mV, respectively. This overpotential value ($-$251 mV) for the nanocomposite is significantly lower than for known MgO-based electrocatalysts [12]. The observed reduction in overpotential of the g-C_3N_4-coated electrodes with the MgO addition can be explained by the higher surface area and morphological features of nanocomposite which promote free removal of evolved hydrogen bubbles (kinetic factor). From the other hand, direct and numerous contact of nanoparticles of the two components (g-C_3N_4 and MgO) leads to the formation of new interfaces, where a redistribution of electron densities occurs, which makes it easier to initiate the hydrogen evolution process (thermodynamic factor). Additional information was obtained using this data recalculation to the Tafel coordinates (so-called Tafel plot), where the Tafel slope indicates a change in overpotential value with a 10-fold increase in current density. Fig. 6(b) presents the results of the voltammogram analysis in the Tafel plot. Tafel slope for g-C_3N_4 and g-C_3N_4/5%MgO samples was found to be equal to

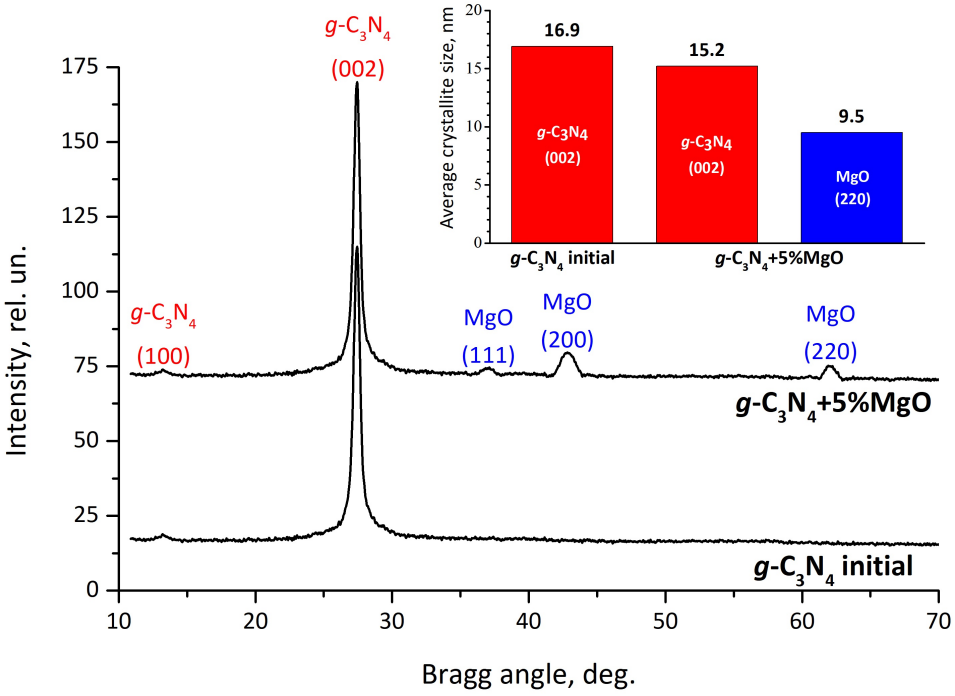

FIG. 5. PXRD patterns of initial g-C_3N_4 and g-C_3N_4/5%MgO nanocomposite and assignment of the main diffraction reflections of graphitic carbon nitride (g-C_3N_4) and magnesia (MgO). The inset shows the average crystallite sizes of g-C_3N_4 and MgO nanocrystals of initial g-C_3N_4 and g-C_3N_4/5%MgO nanocomposite

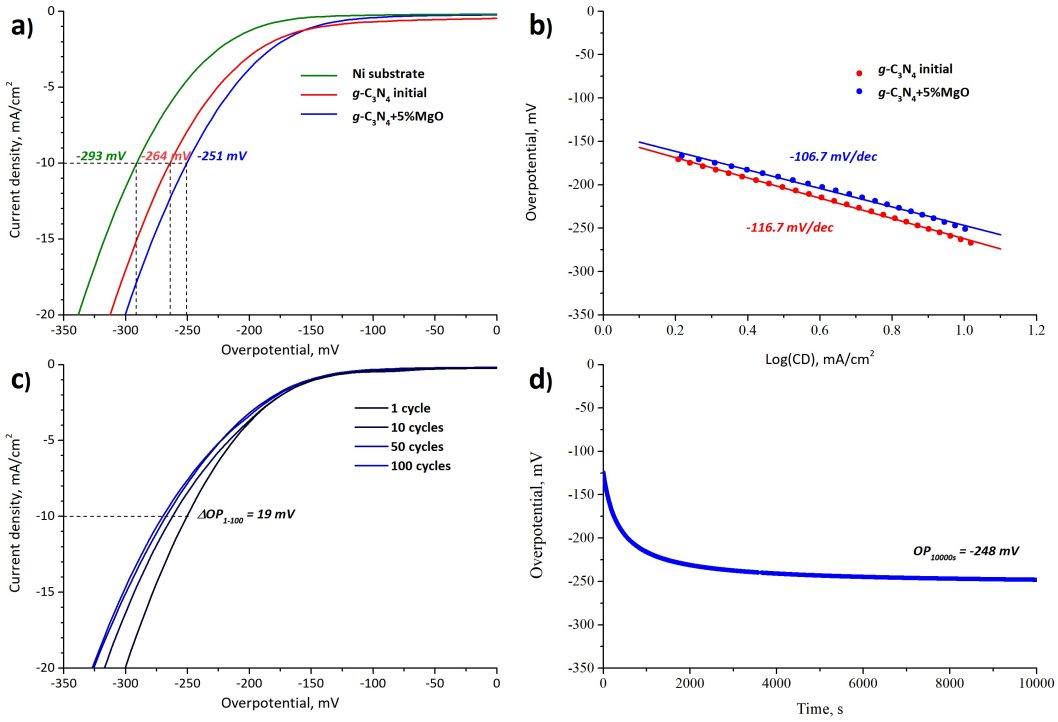

FIG. 6. Electrocatalytic performance of g-C_3N_4/5%MgO nanocomposite in hydrogen production via reforming of water-ethanol (10% vol.) solution: (a) HER polarization curves, (b) Tafel plot, (c) cycling stability, (d) chronopotentiometry stability

116 mV and 106 mV, respectively. Both values are lower than for the pure nickel electrode (120 mV) which provides an economic advantage in electrochemical reforming.

Then, the standard cyclic voltammetry and chronopotentiometry techniques [13, 14] were used to estimate the electrochemical stability of the g-C_3N_4/MgO-based electrode. Fig. 6(c) shows the polarization curves obtained at a sweep rate of 5 mV/s for the g-C_3N_4/5%MgO after 1, 10, 50 and 100 cycles of cyclic voltammetry (CVA). After 100 times cycling of the electrode, the value of overpotential slightly degrades, reaching values of about -270 mV. But, according to the results of chronopotentiometry (Fig. 6(d)), the value of overpotential for g-C_3N_4/MgO sample at a time, when the non-stationary mode ends, is 248 mV. The time-value for this sample is about 2000 s and doesn't change, even after a 10000 s testing. These results of both cyclic voltammetry and chronopotentiometry allow us to declare the high electrochemical stability of the synthesized g-C_3N_4/5%MgO nanocomposite in a water-ethanol reforming process.

4. Conclusion

In summary, a simple wet-chemical approach was proposed and used to synthesize g-C_3N_4/MgO nanocomposite with enhanced electrocatalytic activity compared with pure g-C_3N_4. This approach allowed synthesis of a high chemical and phase purity of g-C_3N_4-based nanocomposite with 5% wt. MgO content, as well as to ensure the uniform distribution of the individual components (g-C_3N_4 and MgO) over the volume of the synthesized electrocatalyst. It was found that the electrochemical characteristics (overpotential, Tafel slope, etc) of the g-C_3N_4/MgO nanocomposite electrode was significantly improved compared to both g-C_3N_4-coated and pure nickel electrode. At the same time, it was shown that the cyclic and chronopotentiometry stabilities of the nanocomposite-coated electrode are at a high and practically significant level. Thus, it was established and confirmed that synthesized g-C_3N_4/5%MgO nanocomposite is an effective and high stable electrode material that seems to be perspective as electrode base for electrocatalytic reforming of a water-alcohol solution toward hydrogen production.

References

[1] Yuan Y., Ruan L., Barber J., Joachim Loo S.C., Xue C., Hetero-nanostructured suspended photocatalysts for solar-to-fuel conversion. *Energy Environ. Sci.*, 2014, **7**, P. 3934–3951.

[2] Cao S., Low J., Yu J., Jaroniec M. Polymeric photocatalysts based on graphitic carbon nitride. *Adv. Mater.*, 2015, **27**, P. 2150–2176.

[3] Wang X., Maeda K., Thomas A., Takanabe K., Xin G., Carlsson J.M., Domen K., Antonietti M. A metal-free polymeric photocatalyst for hydrogen production from water under visible light. *Nat. Mater.*, 2009, **8**, P. 76–80.

[4] Mishra A., Mehta A., Basu S., Shetti N.P., Reddy K.R., Aminabhavi T.M. Graphitic carbon nitride (g-C_3N_4)-based metal-free photocatalysts for water splitting: A review. *Carbon*, 2009, **149**, P. 693–721.

[5] Wen J., Xie J., Chen X., Li X., A review on g-C_3N_4-based photocatalysts. *Appl. Surf. Sci.*, 2017, **391**, P. 72–123.

[6] Sudhaik A., Raizada P., Shandilya P., Jeong D.Y., Lim J.H., Singh P. Review on fabrication of graphitic carbon nitride based efficient nanocomposites for photodegradation of aqueous phase organic pollutants. *J. Ind. Eng. Chem.*, 2018, **67**, P. 28–51.

[7] Mao N., Jiang J.-X., MgO/g-C_3N_4 nanocomposites as efficient water splitting photocatalysts under visible light irradiation. *Appl. Surf. Sci.*, 2019, **476**, P. 144–150.

[8] Chaudhary P., Ingole P.P. In-Situ solid-state synthesis of 2D/2D interface between Ni/NiO hexagonal nanosheets supported on g-C_3N_4 for enhanced photo-electrochemical water splitting. *International Journal of Hydrogen Energy*, 2020, **45**(32), P. 16060–16070.

[9] Chebanenko M.I., Zakharova N.V., Lobinsky A.A., Popkov V.I. Ultrasonic-Assisted Exfoliation of Graphitic Carbon Nitride and its Electrocatalytic Performance in Process of Ethanol Reforming. *Semiconductors*, 2019, **53**(16), P. 28–33.

[10] Chebanenko M.I., Zakharova N.V., Popkov V.I., Synthesis and Visible-Light Photocatalytic Activity of Graphite-like Carbon Nitride Nanopowders. *Russ. J. Appl. Chem.*, 2020, **93**(4), P. 494–501.

[11] Nikolic V.M., Maslovara S.L., Tasic G.S., et al. Kinetics of hydrogen evolution reaction in alkaline electrolysis on a Ni cathode in the presence of Ni-Co-Mo based ionic activators. *Appl. Catal. B Environ.*, 2015, **179**, P. 88–94.

[12] Thomas S., Medhekar N.V., Frankel G.S., Birbilis N. Corrosion mechanism and hydrogen evolution on Mg. *Curr. Opin. Solid St. M.*, 2015, **19**(2), P. 85–94.

[13] Kodintsev I.A., Martinson K.D., Lobinsky A.A., Popkov V.I. SILD synthesis of the efficient and stable electrocatalyst based on CoO–NiO solid solution toward hydrogen production. *Nanosystems: Phys. Chem. Math.*, 2019, **10**(6), P. 681–685.

[14] Dmitriev D.S., Nashchekin A.V., Popkov V.I. The interfacial surface of an electrode for a supercapacitor as a factor affecting the capacitance and energy density. *Appl. Surf. Sci.*, 2020, **501**, P. 144216.